

# Journal of Materials Chemistry A

Accepted Manuscript



This is an *Accepted Manuscript*, which has been through the Royal Society of Chemistry peer review process and has been accepted for publication.

*Accepted Manuscripts* are published online shortly after acceptance, before technical editing, formatting and proof reading. Using this free service, authors can make their results available to the community, in citable form, before we publish the edited article. We will replace this *Accepted Manuscript* with the edited and formatted *Advance Article* as soon as it is available.

You can find more information about *Accepted Manuscripts* in the [Information for Authors](#).

Please note that technical editing may introduce minor changes to the text and/or graphics, which may alter content. The journal's standard [Terms & Conditions](#) and the [Ethical guidelines](#) still apply. In no event shall the Royal Society of Chemistry be held responsible for any errors or omissions in this *Accepted Manuscript* or any consequences arising from the use of any information it contains.

## ARTICLE

## Thermoelectric properties of Sn doped p-type $\text{Cu}_3\text{SbSe}_4$ : a compound with large effective mass and small band gap†

Cite this: DOI: 10.1039/x0xx00000x

Tian-Ran Wei,<sup>†a</sup> Heng Wang,<sup>†b</sup> Zachary M. Gibbs,<sup>b</sup> Chao-Feng Wu,<sup>a</sup> G. Jeffrey Snyder,<sup>b</sup> and Jing-Feng Li<sup>\*a</sup>

Received 00th January 2012,  
Accepted 00th January 2012

DOI: 10.1039/x0xx00000x

www.rsc.org/

$\text{Cu}_3\text{SbSe}_4$ -based compounds composed of earth-abundant elements have been found to exhibit good thermoelectric performance at medium temperature. High  $zT$  values were achieved in previous studies, but further insight into the transport mechanism as well as some key material parameters is still needed. In this work we study the electrical and thermal transport properties of Sn doped  $\text{Cu}_3\text{SbSe}_4$  between 300 K and 673 K. It is found here the single parabolic band model explains the electrical transport very well. Experimentally we determine the band gap to be around 0.29 eV. Density-of-state effective mass is found to be about 1.5  $m_e$  for doped samples. The transport properties suggest a degeneracy splitting near valence band maximum that was not captured by previous band structure calculation. The maximum  $zT \sim 0.70$  is obtained at 673 K and the optimized carrier density is  $\sim 1.8 \times 10^{20} \text{ cm}^{-3}$ . The potential of further improvement of  $zT$  via material engineering is briefly discussed.

### Introduction

Thermoelectric materials which can realize the direct conversion between heat and electricity in the solid state are expected to play a significant role in the field of clean energy development and utilization.<sup>1</sup> Developing materials with high figure of merit,  $zT$ , defined as  $zT = S^2T/\rho\kappa$  ( $S$ ,  $T$ ,  $\rho$  and  $\kappa$  are Seebeck coefficient, absolute temperature, electrical resistivity and thermal conductivity, respectively), has been the main topic of research in thermoelectrics.<sup>2-6</sup> Recently, copper chalcogenides have received increasing attention as promising thermoelectric materials with high  $zT$ , such as superionic  $\text{Cu}_2\text{Se}$ <sup>7-9</sup> with liquid-like phonon behaviour and layered oxyselenide  $\text{BiCuSeO}$ <sup>10-13</sup>. Other high-symmetry ternary or multinary copper chalcogenides composed of Cu-M tetrahedral (M is a chalcogen) bonds include chalcopyrite, tetrahedrite and famatinite, *etc.* Many of these compounds are found to be promising thermoelectrics as well, such as  $\text{CuGaTe}_2$ ,<sup>14, 15</sup>  $\text{CuInTe}_2$ ,<sup>16</sup>  $\text{Cu}_{2.1}\text{Zn}_{0.9}\text{SnSe}_4$ ,<sup>17</sup>  $\text{Cu}_2\text{ZnGeSe}_4$ <sup>18</sup> and  $\text{Cu}_3\text{SbM}_4$  (M = Se, S),<sup>19, 20</sup> even  $\text{Cu}_{12}\text{Sb}_4\text{S}_{13}$  and  $\text{Cu}_{12}\text{As}_4\text{S}_{13}$  right from their natural mineral form<sup>21, 22</sup>. Among these compounds,  $\text{Cu}_3\text{SbSe}_4$  is a p-type semiconductor with a small band gap. Previous investigations have been carried out focusing on adjusting carrier density and forming solid solutions towards high  $zT$ .<sup>23, 24</sup>

In spite of the knowledge that has already been obtained in  $\text{Cu}_3\text{SbSe}_4$ , further insight into the transport mechanism as well as some key material parameters that are essential for further

optimization towards higher  $zT$  is still inadequate. In this work, we take a close look on the transport properties of p-type  $\text{Cu}_3\text{SbSe}_4$ . Our samples are prepared using mechanical alloying and spark plasma sintering. This simple method has led to high quality samples with homogeneous microstructure, nearly ideal doping efficiency and well behaved transport properties. This compound is found to be a semiconductor with a large effective mass about 1.5  $m_e$  (when doped) and a small band gap of  $\sim 0.29$  eV. The transport data also suggest a split of valence bands that was not revealed by previous calculations. These findings provide in-depth understanding of the promising  $zT$  and possible strategies for further material engineering.

### Experimental

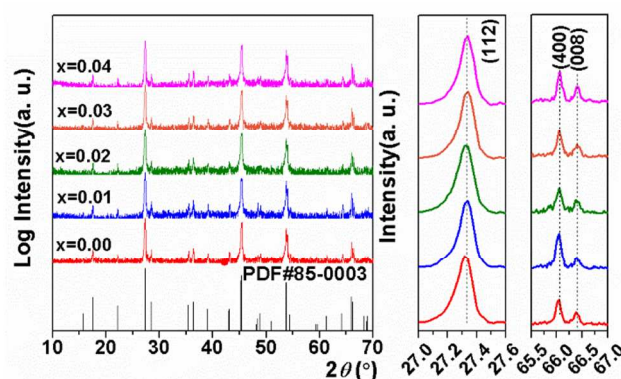
Samples with nominal compositions  $\text{Cu}_{2.95}\text{Sb}_{1-x}\text{Sn}_x\text{Se}_4$  ( $x = 0, 0.01, 0.02, 0.03, 0.04$ ) were fabricated *via* mechanical alloying (MA) and spark plasma sintering (SPS). Cu deficiency is chosen to compensate for Se volatilization and achieve best performance, which was discussed in detail in a previous report.<sup>25</sup> A mixture of Cu, Sb, Sn and Se powders of high purity were milled in a stainless steel vessel on a planetary ball mill at 425 rpm for 10 hours protected by a mixed atmosphere of 95 vol% Ar and 5 vol%  $\text{H}_2$  gases, and then were milled in an alcohol solution. The as-synthesized powders were sintered by SPS at 703 K for 5 min under a uniaxial pressure of 50 MPa

into disk-shaped samples about 3 mm in thickness and about 93% or higher in relative density.

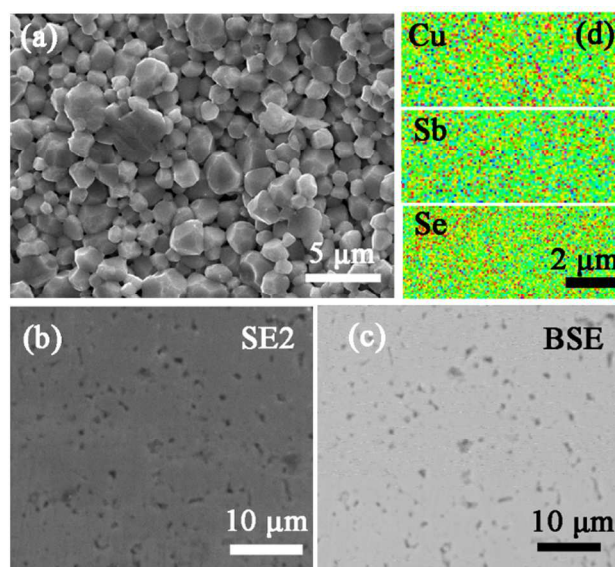
The phase structures were investigated by X-ray diffraction (XRD) with a D/max-RB diffractometer (Rigaku, Japan) using Cu  $K\alpha$  radiation. Scanning electron microscopy (SEM) images of the bulk materials were taken in the secondary electron detector (SE2) mode and the backscattering electron (BSE) mode by field emission scanning electron microscopy (FE-SEM, JSM-7001, JEOL, Japan). Electronic probe microscopic analysis (EPMA, JXA-8230, JEOL, Japan) was used to analyze the ratio and distribution of the elements on polished surface of bulk samples. Bar-shaped specimens were cut along the radial direction of a disk sample for measurement of the Seebeck coefficient ( $S$ ) and the electrical resistivity ( $\rho$ ) as functions of temperature, using a Seebeck coefficient/electric resistance measuring system (ZEM-2, Ulvac-Riko, Japan). Hall coefficient ( $R_H$ ) at and above 300 K was measured under a reversible magnetic field by the Van der Pauw technique using a Hall measurement system (8340DC, Toyo, Japan). The Hall carrier density ( $n_H$ ) was calculated via  $n_H = 1/(eR_H)$ , and the Hall carrier mobility ( $\mu_H$ ) was obtained using the relationship  $\mu_H = R_H/\rho$ . The thermal diffusivity ( $D$ ) was measured in the thickness direction of a disk-shaped sample of  $\phi$  10 mm and about 1.5 mm in thickness using a laser flash diffusivity method (TC9000, Ulvac-Riko, Japan). The specific heat capacity ( $C_p$ ) was measured by the Quantum Design physical property measurement system (PPMS) as well as the Netsch LFA 457 laser flash thermoanalysis system. Thermal conductivity ( $\kappa$ ) was calculated by  $\kappa = D \cdot C_p \cdot d$ , where  $d$  is the density measured by the Archimedes method. Optical absorption edge measurements were carried out on the undoped sample using a Nicolet 6700 FTIR Spectrophotometer equipped with a Praying Mantis Diffuse Reflectance attachment (Harrick Scientific Instruments) at room temperature and up to 573 K. The scans were referenced to KBr standard samples. Optical gaps were obtained by extrapolating  $\alpha$ , the absorption coefficient, to 0 as a function of  $(h\nu)^n$ , where  $h\nu$  is the photon energy, and  $n$  is equal to 2 for direct gaps, 0.5 for indirect gaps.

## Results and discussion

The XRD patterns of the samples subjected to SPS are shown in Fig. 1, which suggest single phase  $\text{Cu}_3\text{SbSe}_4$  (PDF #85-0003) regardless of Sn content. No peak shift even at high angles was found with the doping of Sn, due to the small difference in ionic size<sup>26</sup> between  $\text{Sn}^{4+}$  and  $\text{Sb}^{5+}$  and the low doping level. The morphology of fractured and polished surfaces for a representative sample of  $\text{Cu}_{2.95}\text{Sb}_{0.98}\text{Sn}_{0.02}\text{Se}_4$  is shown in Fig. 2. The fractured surface exhibits well crystallized grains with an average grain size of  $\sim 2 \mu\text{m}$ . The back scattering electron (BSE) graph and EPMA mapping confirmed a homogeneous distribution of elements without segregation of secondary phases.

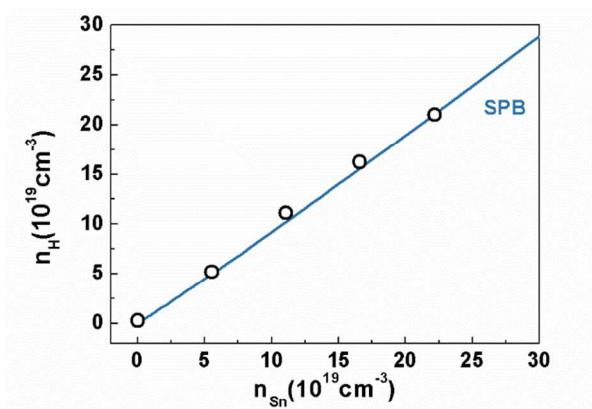


**Fig. 1** XRD patterns of  $\text{Cu}_{2.95}\text{Sb}_{1-x}\text{Sn}_x\text{Se}_4$ , no peak shift due to doping of Sn can be seen.



**Fig. 2** Morphology and elemental distribution of bulk  $\text{Cu}_{2.95}\text{Sb}_{0.98}\text{Sn}_{0.02}\text{Se}_4$ : (a) SE2 image of fractured surface; (b) SE2 image, (c) BSE image and (d) EPMA mapping of main elements of polished surface.

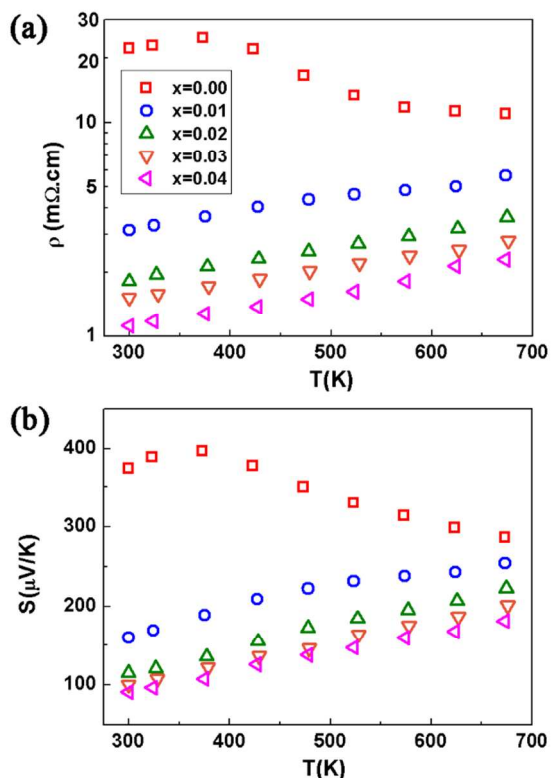
Undoped  $\text{Cu}_3\text{SbSe}_4$  is an intrinsic semiconductor with carrier density on the order of  $10^{18} \text{cm}^{-3}$ . Substituting Sn for Sb continuously increases carrier density up to  $2 \times 10^{20} \text{cm}^{-3}$ . There has been debate on the specific valence number of Sb in  $\text{Cu}_3\text{SbSe}_4$ , both 5+ and 3+ have been suggested.<sup>27-29</sup> Nonetheless with a simple argument that Sn has one less valence electron than Sb and is tetrahedrally bonded just as Sb in the structure, each Sn is expected to donate one free hole. This trend is well followed for samples studied here, as shown in Fig. 3: the measured Hall carrier density  $n_H$  at room temperature follows exactly the calculated result (solid line) based on the density of substitutional Sn atoms assuming each of them contribute one free hole, using the single parabolic band (SPB) model (which determines Hall factor  $r_H$  that links  $n_H$  with the chemical carrier density  $n$  via  $n_H = n/r_H$ ).



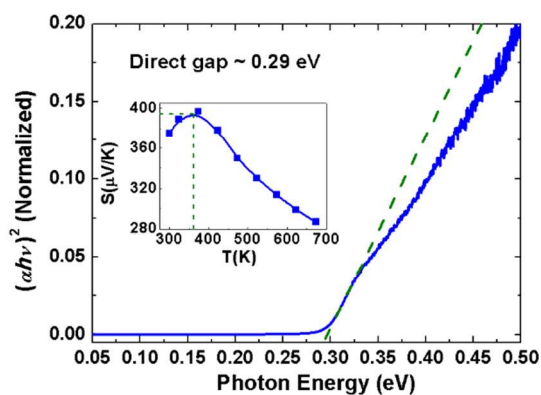
**Fig. 3** Hall carrier density as a function of dopant density at room temperature. The solid line is calculated by SPB assuming each Sn donates one free hole.

Fig. 4 shows the electrical resistivity ( $\rho$ ) and Seebeck coefficient ( $S$ ) as functions of temperature. All the samples show p-type character. The undoped sample exhibits a nondegenerate behavior with relatively large and decreasing Seebeck coefficient and resistivity with increasing temperature. From  $S$  of the undoped sample the band gap  $E_g$  was estimated to be about 0.29 eV *via*<sup>30</sup>

$$E_g = 2eS_{\max}T_{S_{\max}} \quad (1)$$



**Fig. 4** (a) Electrical resistivity and (b) Seebeck coefficient as functions of temperature.



**Fig. 5** Band gap by optical absorption edge measurements in undoped  $\text{Cu}_3\text{SbSe}_4$ .

This estimate is consistent with the band gap measured by optical absorption spectrum, which indicated a clear direct transition at 0.29 eV, shown in Fig. 5. Previously a similar band gap was reported by Berger *et al.* using optical method.<sup>31</sup> We have also noticed that a much smaller gap of 0.13 eV was suggested by Nakanishi *et al.* by analyzing temperature dependence of electrical resistivity and Hall coefficient, and 0.11 eV *via* infrared transmission spectra.<sup>32</sup> Similar value was also obtained by Li *et al.* by fitting electrical resistivity against temperature.<sup>33</sup> In fact, we found a similar activation energy of  $\Delta E \sim 0.13$  eV in this study by fitting the linear relation  $\ln\rho-1/T$  from the undoped sample. Further, our optical absorption has shown a very weak absorption above 0.12 eV, possibly corresponding to an indirect transition. However, we conclude here that the activation energy of 0.12 eV is not likely to be the primary band gap, because the large  $S$  values in undoped samples would not be achievable. In order to maintain a high Seebeck coefficient ( $\sim 400\mu\text{V/K}$  at  $\sim 300\text{K}$ ) the chemical potential needs to be deep in the gap, while a small gap of 0.12 eV would inevitably induce significant minority carriers that compensate the Seebeck value. As a result, the band gap is believed to be 0.29 eV corresponding to the direct transition, which is several orders of magnitude stronger than the supposed indirect transition. The activation energy of 0.12 eV is then speculated to be due to defect levels inside the band gap. Nakanishi *et al.* were not able to observe the much stronger direct transition because they used optical transmission which had already been saturated to zero throughput after the first indirect transition at 0.12 eV. A band gap around 0.3 eV is comparable with other good thermoelectrics such as  $\text{PbTe}$ <sup>34-36</sup> or  $\text{PbSe}$ <sup>37-39</sup>,  $\text{Mg}_2\text{Si}_{0.4}\text{Sn}_{0.6}$ <sup>40</sup> and  $\text{ZrNiSn}$ <sup>41</sup>. Small band gaps usually mean less ionic character making it easier for delocalized charge carriers that lead to high mobilities desirable for thermoelectrics. The disadvantage of a small band gap is the tendency of excitation of minority carriers.

The measured Hall mobility  $\mu_H$  for all samples decreases with temperature (Fig. 6 (a)). Near room temperature the  $T^{-3/2}$  law is roughly obeyed by all samples, indicating the dominance of acoustic phonon scattering of carriers. Fig. 6 (b) shows the measured  $n_H$  at different temperatures. For each doped sample  $n_H$  remains constant near room temperature and above 500 K it increases slowly with

temperature. Given a small and temperature independent  $E_g = 0.29$  eV in  $\text{Cu}_3\text{SbSe}_4$  the apparent increase of  $n_H$  is likely due to bipolar excitation.

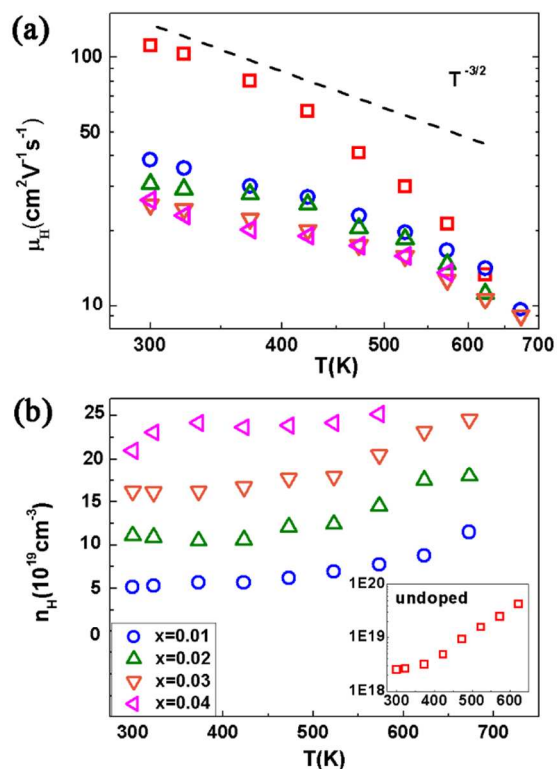


**Fig. 6** (a) Hall mobility and (b) Hall carrier density as functions of temperature for  $\text{Cu}_{2.95}\text{Sb}_{1-x}\text{Sn}_x\text{Se}_4$ . The Hall carrier density of the undoped sample is depicted in the inset of (b).

Fig. 7 shows the carrier density dependence of the Seebeck coefficient and Hall mobility at room temperature, together with data previously reported for this system<sup>23, 33, 42</sup>. We found that the SPB model with acoustic phonon scattering assumption could well explain both properties. From the carrier density dependence of Seebeck coefficient (the Pisarenko relation), it seems that all measured  $S$  are consistent with a constant density-of-state (DOS) effective mass,  $m^* = 1.5 m_e$ . However, a range of  $m^*$  values from 1.1  $m_e$  and 1.7  $m_e$  are acceptable. In fact, by calculating  $m^*$  for each individual sample we found a clear increase when going from undoped to doped samples (inset of Fig. 7 (a), error bars are estimated assuming 5% uncertainty in  $S$  measurement that is normally seen). Large effective mass usually means less mobile carriers and lower thermoelectric quality factor defined as:

$$B = \frac{2k_B^2 \hbar}{3\pi} \frac{dv_l^2 N_V}{m_l^* \Xi^2 \kappa_L} T \quad (2)$$

where  $v_l$  is the longitudinal speed of sound,  $d$  is the density,  $N_V$  is the degeneracy of band,  $m_l^*$  is the inertial effective mass,  $\kappa_L$  is the lattice thermal conductivity and  $\Xi$  is the deformation potential coefficient.<sup>43</sup> In the case of  $\text{Cu}_3\text{SbSe}_4$ , however, the large  $m^*$  comes from three bands that are degenerate (suggested by calculation<sup>29</sup>) at valence band maximum. As known in lead chalcogenides, large effective

mass from highly degenerate bands is favourable for high thermoelectric performance.<sup>35</sup>

The changing  $m^*$  with doping level is also indicated by the carrier density dependence of the Hall mobility  $\mu_H$ . In the SPB model,  $\mu_H$  of a system with reduced chemical potential  $\eta$  can be expressed as<sup>43</sup>:

$$\mu_H = \frac{3\sqrt{\pi}}{8} \mu_0 \frac{F_{-1/2}(\eta)}{F_0(\eta)} = \frac{\pi e \hbar^4 dv_l^2 N_V^{5/3}}{2\sqrt{2} m^{*5/2} (k_B T)^{3/2} \Xi^2} \frac{F_{-1/2}(\eta)}{F_0(\eta)} \quad (3)$$

$$F_n(\eta) = \int_0^\infty \frac{x^n dx}{1 + \exp(x - \eta)} \quad (4)$$

Where  $\mu_0$  is the nondegenerate limit of mobility governed by acoustic phonon scattering process. We found that for doped samples the SPB model provides a good fit with  $\mu_0$  determined to be 49  $\text{cm}^2\text{V}^{-1}\text{s}^{-1}$ . The measured mobility of undoped sample on the other hand, is about twice as high as this value. We notice that all available reports<sup>23, 33, 42</sup> on undoped samples agree with our finding. Furthermore for the sample studied in this work, this result is repeatable in at least two measurements from room temperature to 673 K. So the high mobilities are unlikely due to measurement error or non-equilibrium conditions. Using SPB model, the difference can be well explained by the variation in effective mass considering  $m^*$  is 1.1  $m_e$  for the undoped sample and 1.5  $m_e$  for doped ones, as suggested by inset of Fig. 7 (a).

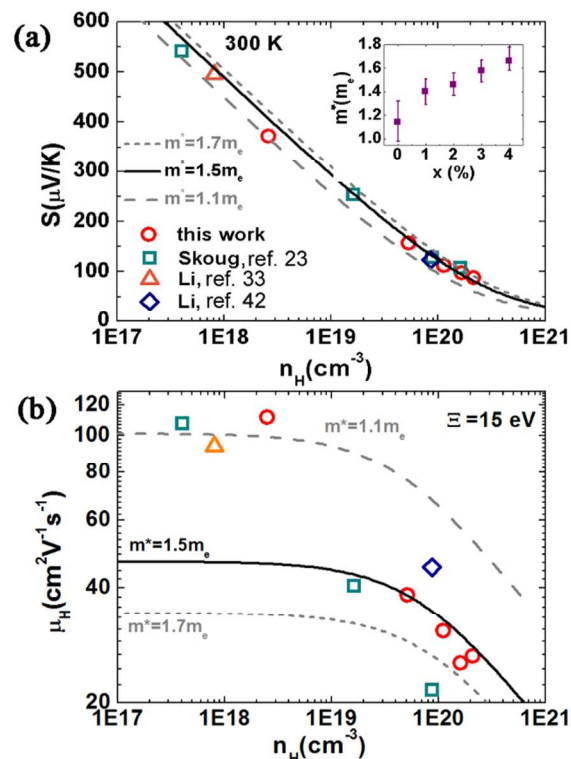


**Fig. 7** Change of (a) Seebeck coefficient and (b) Hall mobility with Hall carrier density at room temperature. The inset of (a) shows the effective mass for each sample determined from  $S$  and  $n_H$ .

Previous band structure calculation for  $\text{Cu}_3\text{SbSe}_4$  suggested a maximum of valence band at  $\Gamma$  point where three bands with

different effective masses are degenerate.<sup>29</sup> The observed Pisarenko relation at 300 K, however, clearly imply changing effective masses that can't be explained by multiply degenerate bands. The observed transport properties instead suggest a split of at least two of these three bands near the maximum, possibly due to the spin-orbit coupling which was not taken into account in the reported calculation. Consequently, as the chemical potential moves deep into the valence bands with the increase of carrier density, the secondary bands begin to play a more noticeable role in transport leading to a larger  $m^*$  when the system is characterized with the SPB model.

While the observed Pisarenko relation and changing effective mass with increased doping level can be simply explained by the split of bands near the valence band maximum, the carrier density dependence of mobility (seen in Fig. 7 (b)) requires more complicated physics to fully understand. Even with the band configuration, one would not expect the trend in Fig. 7 (b) without allowing inter-band scattering or additional scattering mechanisms associated with increased density of dopants. Nonetheless, for the doped samples which are of most interest to thermoelectrics, the SPB model with acoustic phonon scattering assumption still provides an effective way to understand the transport properties. With reported  $v_l$  of 3643 m/s,<sup>27</sup> and assuming  $N_V = 3$ ,<sup>29</sup> the deformation potential coefficient  $\Xi$ , was found to be  $15 \pm 0.5$  eV at 300 K. This value is smaller than those found in systems with smaller effective mass such as lead chalcogenides<sup>44, 45</sup> and  $\text{Bi}_2\text{Te}_3$ <sup>46</sup>, whereas it is noticeably larger when compared with systems with larger effective mass ( $>1 m_e$  for a single valley) such as  $\text{La}_3\text{Te}_4$ <sup>47</sup>,  $\text{Yb}_{14}\text{MnSb}_{11}$ <sup>48</sup> and  $\text{ZrNiSn}$ <sup>49</sup>.

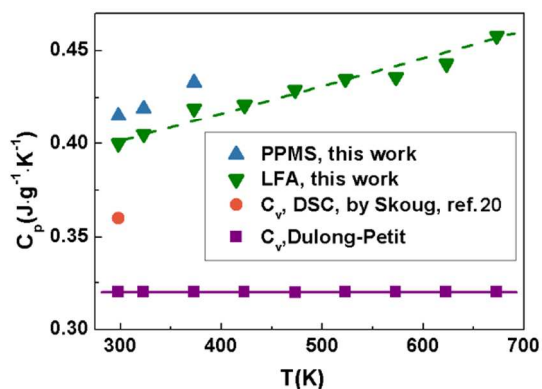


**Fig. 8** Heat capacity as a function of temperature for undoped  $\text{Cu}_3\text{SbSe}_4$ . Skoug's result is  $1.85 \text{ Jcm}^{-3}\text{K}^{-1}$  in ref. 20 and is converted to be  $0.36 \text{ Jg}^{-1}\text{K}^{-1}$  by assuming the relative density to be 90%.

To determine the thermal conductivity of the samples,  $C_p$  was measured between 300 K and 673 K and the values are shown in Fig. 8. We notice that the measured results from two different instruments, while consistent with each other, are considerably higher than the Dulong-Petit  $C_V$ . Above the Debye temperature (131 K by Berger *et al.*<sup>31</sup>, 60-80 K by Zhang *et al.*<sup>27</sup> and 65 K by Skoug *et al.*<sup>50</sup>)  $C_p$  for solids is generally larger than  $C_V$  due to lattice

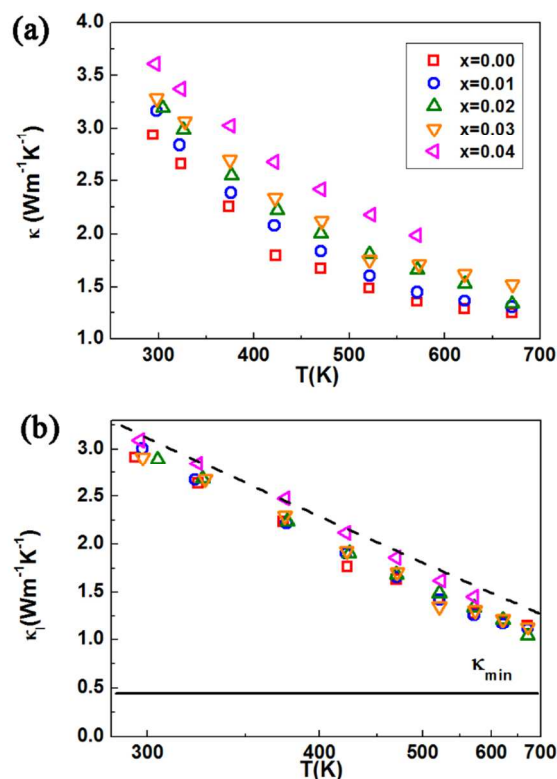


**Fig. 9** (a) Total thermal conductivity and (b) lattice thermal conductivity as functions of temperature.

expansion. While this qualitatively explains the linear increase of  $C_p$  with temperature, the difference at room temperature (20%) is much larger than one would expect. The difficulty in accurate determination of  $C_p$  experimentally and thus the different values used by different studies is partially responsible for the difference in reported  $zT$  values.

Fig. 9 shows the total thermal conductivity and the lattice thermal conductivity as functions of temperature. The electronic thermal conductivity  $\kappa_e$  was calculated by  $\kappa_e = LT/\rho$ , where the Lorenz number  $L$ , was calculated with the SPB model. The lattice thermal conductivity  $\kappa_L$  decreases with temperature following  $T^{-1}$  (dashed line), which indicates the dominance of phonon-phonon Umklapp scattering in phonon transport. Even in the undoped sample,  $\kappa_L$  decreases with  $T$  in the whole measurement range, and no obvious bipolar contribution was observed. Due to the low percentage of Sn substitution and the small size difference between Sb and Sn, no difference in  $\kappa_L$  between doped and undoped samples is observed. The minimum lattice thermal conductivity for  $\text{Cu}_3\text{SbSe}_4$ ,  $\kappa_{min}$ , was estimated using Cahill's formula<sup>51</sup> and was found to be around  $0.47 \text{ Wm}^{-1}\text{K}^{-1}$  from 275 K to 700 K. Experimentally  $\kappa_L$  found at 673 K is around  $1.1 \text{ Wm}^{-1}\text{K}^{-1}$ , so further reduction of  $\kappa_L$  is possible.

The figure of merit,  $zT$ , is shown as a function of temperature in Fig. 10 (a). The maximum value  $\sim 0.70$  was reached at 673 K in the sample with 2% Sn doping, and the corresponding Hall carrier density is  $\sim 1.8 \times 10^{20} \text{ cm}^{-3}$ . We further calculated  $zT$  as a function of  $n_H$  from the SPB model using parameters for doped samples

determined at 300 K. The result is shown in Fig. 10 (b). The optimal carrier density corresponding to the highest  $zT$  increases from  $\sim 4.5 \times 10^{19} \text{ cm}^{-3}$  at 300 K to  $\sim 1.2 \times 10^{20} \text{ cm}^{-3}$  at 673 K, as demonstrated experimentally and theoretically. According to the modeling, significantly higher  $zT$  than 0.7 is not likely for  $\text{Cu}_3\text{SbSe}_4$  just by tuning the carrier density. Two possible routes to higher  $zT$  via material engineering are: first by tuning the position of individual valence bands so they are better aligned at the maximum; and second by forming solid solutions that reduces  $\kappa_L$ . It should be noted that at high temperatures  $\text{Cu}_3\text{SbSe}_4$  has an inherent  $\kappa_L$  only twice as high as the theoretical minimum (comparable to the case of  $\text{PbTe}$  or  $\text{PbSe}$  where  $\kappa_L$  is around  $0.7 \text{ Wm}^{-1}\text{K}^{-1}$  and  $\kappa_{\text{min}}$  is around  $0.4 \text{ Wm}^{-1}\text{K}^{-1}$ ), and that forming solid solution will also decrease the carrier mobility, so forming solid solutions would likely increase  $zT$  but not significantly. Actually the  $zT$  value reported for  $\text{Cu}_3\text{SbSe}_{4-x}\text{S}_x$  is 0.89: about 20% increase over that of  $\text{Cu}_3\text{SbSe}_4$  reported by the same group.<sup>20, 23</sup>

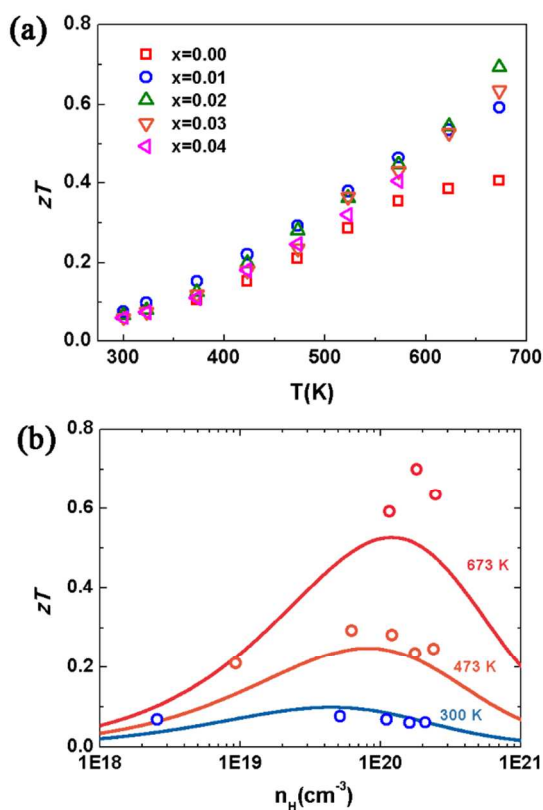


**Fig. 10**  $zT$  as a function of (a) temperature and (b) Hall carrier density for Sn-doped  $\text{Cu}_3\text{SbSe}_4$ . Solid curves were calculated with SPB model using parameters for doped samples determined at 300 K.

## Conclusions

Polycrystalline  $\text{Cu}_3\text{SbSe}_4$  doped with Sn were fabricated with high phase purity and precisely controlled carrier density using mechanical alloying and spark plasma sintering. The transport behaviour of this compound was explained by the single parabolic band (SPB) model. The Seebeck coefficients and mobilities at 300 K

of samples with different doping levels suggested a split of bands at the valence band maximum, which according to previous calculation are triply degenerate. Transport data and optical band gap measurements suggested a direct band gap  $\sim 0.29 \text{ eV}$  that is temperature independent. Thermal conductivity was governed by the Umklapp phonon scattering and a  $T^{-1}$  dependence was observed for all samples. The maximum  $zT$  value  $\sim 0.70$  was obtained at 673 K with 2% Sn (Hall carrier density  $1.8 \times 10^{20} \text{ cm}^{-3}$ ). The analyses and findings in this study would potentially help the understanding of transport properties in similar Cu-based ternary or multinary thermoelectric materials.

## Acknowledgements

This work was supported by National Natural Science Foundation (No. 51172121) and the National Basic Research Program of China (Grant No. 2013CB632503) as well as 863 Program under Grant No. 2012AA051104. H. W., Z. M. G and G. J. S. acknowledge the support from the AFOSR MURI program in USA and the Molecular Materials Research Center (MMRC) at Caltech for optical measurement instruments.

## Notes and references

<sup>a</sup> State Key Laboratory of New Ceramics and Fine Processing, School of Materials Science and Engineering, Tsinghua University, Beijing 100084, China. \*E-mail: jingfeng@mail.tsinghua.edu.cn; Fax: +86-62771160; Tel: +86-10-62784845.

<sup>b</sup> Materials Science, California Institute of Technology, Pasadena, CA 91125, USA.

† Electronic Supplementary Information (ESI) available: Enlarged XRD patterns and calculation of the Lorenz number.

‡ Tian-Ran Wei and Heng Wang contributed equally to this work.

- 1 L. E. Bell, *Science*, 2008, **321**, 1457-1461.
- 2 G. J. Snyder and E. S. Toberer, *Nat. Mater.*, 2008, **7**, 105-114.
- 3 J. R. Sootsman, D. Y. Chung and M. G. Kanatzidis, *Angew. Chem. Int. Ed. Engl.*, 2009, **48**, 8616-8639.
- 4 J.-F. Li, W.-S. Liu, L.-D. Zhao and M. Zhou, *NPG Asia Mater.*, 2010, **2**, 152-158.
- 5 J. Yang, H.-L. Yip and A. K.-Y. Jen, *Adv. Energy Mater.*, 2013, **3**, 549-565.
- 6 M. Zebarjadi, K. Esfarjani, M. S. Dresselhaus, Z. F. Ren and G. Chen, *Energy Environ. Sci.*, 2012, **5**, 5147-5162.
- 7 H. Liu, X. Shi, F. Xu, L. Zhang, W. Zhang, L. Chen, Q. Li, C. Uher, T. Day and G. J. Snyder, *Nat. Mater.*, 2012, **11**, 422-425.
- 8 H. Liu, X. Yuan, P. Lu, X. Shi, F. Xu, Y. He, Y. Tang, S. Bai, W. Zhang, L. Chen, Y. Lin, L. Shi, H. Lin, X. Gao, X. Zhang, H. Chi and C. Uher, *Adv. Mater.*, 2013, **25**, 6607-6612.
- 9 D. R. Brown, T. Day, K. A. Borup, S. Christensen, B. B. Iversen and G. J. Snyder, *APL Mater.*, 2013, **1**, 052107.
- 10 L. D. Zhao, D. Berardan, Y. L. Pei, C. Byl, L. Pinsard-Gaudart and N. Dragoe, *Appl. Phys. Lett.*, 2010, **97**, 092118.
- 11 J.-L. Lan, Y.-C. Liu, B. Zhan, Y.-H. Lin, B. Zhang, X. Yuan, W. Zhang, W. Xu and C.-W. Nan, *Adv. Mater.*, 2013, **25**, 5086-5090.
- 12 J. Sui, J. Li, J. He, Y.-L. Pei, D. Berardan, H. Wu, N. Dragoe, W. Cai and L.-D. Zhao, *Energy Environ. Sci.*, 2013, **6**, 2916-2920.

- 13 F. Li, J.-F. Li, L.-D. Zhao, K. Xiang, Y. Liu, B.-P. Zhang, Y.-H. Lin, C.-W. Nan and H.-M. Zhu, *Energy Environ. Sci.*, 2012, **5**, 7188-7195.
- 14 J. Cui, Y. Li, Z. Du, Q. Meng and H. Zhou, *J. Mater. Chem. A*, 2013, **1**, 677-683.
- 15 J. Zhang, X. Qin, D. Li, H. Xin, C. Song, L. Li, X. Zhu, Z. Wang, G. Guo and L. Wang, *J. Mater. Chem. A*, 2014, **2**, 2891-2895.
- 16 R. Liu, L. Xi, H. Liu, X. Shi, W. Zhang and L. Chen, *Chem. Commun.*, 2012, **48**, 3818-3820.
- 17 M.-L. Liu, F.-Q. Huang, L.-D. Chen and I. W. Chen, *Appl. Phys. Lett.*, 2009, **94**, 202103.
- 18 W. G. Zeier, Y. Pei, G. Pomrehn, T. Day, N. Heinz, C. P. Heinrich, G. J. Snyder and W. Tremel, *J. Am. Chem. Soc.*, 2013, **135**, 726-732.
- 19 D. Li, R. Li, X.-Y. Qin, J. Zhang, C.-J. Song, L. Wang and H.-X. Xin, *CrystEngComm*, 2013, **15**, 7166-7170.
- 20 E. J. Skoug, J. D. Cain and D. T. Morelli, *Appl. Phys. Lett.*, 2011, **98**, 261911.
- 21 X. Lu, D. T. Morelli, Y. Xia, F. Zhou, V. Ozolins, H. Chi, X. Zhou and C. Uher, *Adv. Energy Mater.*, 2013, **3**, 342-348.
- 22 X. Lu and D. T. Morelli, *Phys. Chem. Chem. Phys.*, 2013, **15**, 5762-5766.
- 23 E. J. Skoug, J. D. Cain, P. Majsztirik, M. Kirkham, E. Lara-Curzio and D. T. Morelli, *Sci. Adv. Mater.*, 2011, **3**, 602-606.
- 24 C. Yang, F. Huang, L. Wu and K. Xu, *J. Phys. D: Appl. Phys.*, 2011, **44**, 295404.
- 25 T.-R. Wei, F. Li and J.-F. Li, *J. Electron. Mater.*, 2014, **43**, 2229-2238.
- 26 R. D. Shannon, *Acta Crystallogr., Sect. A: Cryst. Phys., Diffraction, Theor. Gen. Crystallogr.*, 1976, **32**, 751-767.
- 27 Y. Zhang, E. Skoug, J. Cain, V. Ozoliņš, D. Morelli and C. Wolverton, *Phys. Rev. B: Condens. Matter Mater. Phys.*, 2012, **85**, 054306.
- 28 E. J. Skoug and D. T. Morelli, *Phys. Rev. Lett.*, 2011, **107**, 235901.
- 29 D. Do, V. Ozolins, S. D. Mahanti, M.-S. Lee, Y. Zhang and C. Wolverton, *J. Phys.: Condens. Matter*, 2012, **24**, 415502.
- 30 H. J. Goldsmid and J. W. Sharp, *J. Electron. Mater.*, 1999, **28**, 869-872.
- 31 L. I. Berger and V. D. Prochukhan, *Ternary Diamond-Like Semiconductors*, Consultants Bureau, New York, 1969.
- 32 H. Nakanishi, S. Endo and T. Irie, *Jpn. J. Appl. Phys.*, 1969, **8**, 443-449.
- 33 X. Y. Li, D. Li, H. X. Xin, J. Zhang, C. J. Song and X. Y. Qin, *J. Alloys Compd.*, 2013, **561**, 105-108.
- 34 Y. I. Ravich, B. A. Efimova and I. A. Smirnov, *Semiconducting Lead Chalcogenides*, Plenum, New York, 1970.
- 35 Y. Pei, X. Shi, A. D. LaLonde, H. Wang, L. Chen and G. J. Snyder, *Nature*, 2011, **473**, 66-69.
- 36 Z. M. Gibbs, A. D. LaLonde and G. J. Snyder, *New J. Phys.*, 2013, **15**, 075020.
- 37 H. Wang, Z. M. Gibbs, Y. Takagiwa and G. J. Snyder, *Energy Environ. Sci.*, 2014, **7**, 804-811.
- 38 Z. M. Gibbs, H. Kim, H. Wang, R. L. White, F. Drymiotis, M. Kaviani and G. Jeffrey Snyder, *Appl. Phys. Lett.*, 2013, **103**, 262109.
- 39 H. Wang, Y. Pei, A. D. LaLonde and G. J. Snyder, *Adv. Mater.*, 2011, **23**, 1366-1370.
- 40 W. Liu, X. Tan, K. Yin, H. Liu, X. Tang, J. Shi, Q. Zhang and C. Uher, *Phys. Rev. Lett.*, 2012, **108**, 166601.
- 41 Q. Shen, L. Chen, T. Goto, T. Hirai, J. Yang, G. P. Meisner and C. Uher, *Appl. Phys. Lett.*, 2001, **79**, 4165.
- 42 D. Li, R. Li, X.-Y. Qin, C.-J. Song, H.-X. Xin, L. Wang, J. Zhang, G.-L. Guo, T.-H. Zou, Y.-F. Liu and X.-G. Zhu, *Dalton Trans.*, 2014, **43**, 1888-1896.
- 43 H. Wang, Y. Pei, A. D. LaLonde and G. J. Snyder, in *Thermoelectric Nanomaterials: Materials Design and Applications*, ed. K. Koumoto and T. Mori, Springer, Heidelberg, 2013, pp. 3-32.
- 44 H. Wang, Y. Pei, A. D. LaLonde and G. J. Snyder, *Proc. Natl. Acad. Sci. U. S. A.*, 2012, **109**, 9705-9709.
- 45 H. Wang, E. Schechtel, Y. Pei and G. J. Snyder, *Adv. Energy Mater.*, 2013, **3**, 488-495.
- 46 B.-L. Huang and M. Kaviani, *Phys. Rev. B: Condens. Matter Mater. Phys.*, 2008, **77**, 125209.
- 47 A. F. May, J.-P. Fleurial and G. J. Snyder, *Phys. Rev. B: Condens. Matter Mater. Phys.*, 2008, **78**, 125205.
- 48 E. S. Toberer, C. A. Cox, S. R. Brown, T. Ikeda, A. F. May, S. M. Kauzlarich and G. J. Snyder, *Adv. Funct. Mater.*, 2008, **18**, 2795-2800.
- 49 H. Xie, H. Wang, Y. Pei, C. Fu, X. Liu, G. J. Snyder, X. Zhao and T. Zhu, *Adv. Funct. Mater.*, 2013, **23**, 5123-5130.
- 50 E. J. Skoug, J. D. Cain, D. T. Morelli, M. Kirkham, P. Majsztirik and E. Lara-Curzio, *J. Appl. Phys.*, 2011, **110**, 023501.
- 51 D. G. Cahill, S. K. Watson and R. O. Pohl, *Phys. Rev. B: Condens. Matter Mater. Phys.*, 1992, **46**, 6131-6140.

Sn-doped  $\text{Cu}_3\text{SbSe}_4$  with enhanced  $zT$  possesses large effective mass, small band gap and moderate deformation potential with complex band structure.

